Numerical analysis of a non-linear energy sink (NES) for the parametric excitation of a submerged cylinder

<u>Guilherme Rosa Franzini</u>, Beatriz Sayuri Sato, Giovanna Ribeiro Campedelli
Offshore Mechanics Laboratory, Escola Politécnica, University of São Paulo, Brazil

<u>*Summary*</u>. This paper addresses passive suppression of oscillations caused by parametric excitation of a rigid and submerged cylinder mounted on an elastic support. A rigid bar, hinged at the axis of the cylinder and with a tip mass is used as a passive absorber, herein named non-linear energy sink (NES). A two degrees-of-freedom analytical model is derived and numerically integrated. The influence of three dimensionless parameters of the mathematical model on the suppression is discussed. The results show that this passive absorber can lead to a marked decrease in the cylinder's oscillation.

Introduction

Passive suppression is a very common subject in dynamics of structures. There are numerous works in this theme for several technological applications. A particular kind of passive absorber consists on a rigid bar, with one extremity pinned at the structure and with a tip-mass. In this paper, such a passive absorber is named as non-linear energy sink (NES), following the nomenclature adopted in [1].

This kind of absorber leads to very interesting dynamic behavior, as documented in several articles. Among interesting aspects, it can be highlighted the presence of non-synchronous oscillations - [2], [3].

Returning to reference [1], the authors investigated the behavior of this kind of suppressor in the mitigation of vortex-induced vibration phenomenon (VIV). Among other findings, it can be highlighted the presence of chaotic response. It is worth to emphasize that similar passive vibration absorbers for VIV, but based on translational displacements of internal masses, are described in references [4] and [5].

The present paper focuses on the use of a NES as a passive absorber for the oscillations caused by parametric excitation of a circular and submerged cylinder. In the next Section, the mathematical model is derived. Following, some numerical results are presented and the main conclusions are addressed.

Mathematical model

Consider the problem sketched in Fig. 1. The rigid cylinder has diameter D and total mass *per* unit length M (including both the structural mass m_s and the potential added mass m_a) and is assembled to an elastic support with time-dependent stiffness $k(t) = \bar{k} + \Delta k \sin \Omega t$ and damping constant c.

Internally to the rigid cylinder, there is a rotating passive absorber, hinged at the axis of the cylinder and composed by a rigid and imponderable bar, with a lumped mass m at its tip. Associated to this passive absorber, there are a rotational spring with stiffness k_θ and a dashpot with damping constant c_θ. The system is immersed on a fluid with density ρ and the gravitational acceleration is parallel to the cylinder axis.
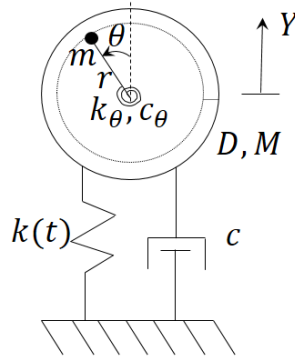
Figure 1: Sketch of the problem.

By applying, for example, Euler-Lagrange's equations, we can easily find the equations of motion of this system:

$$(M + m)\frac{d^2Y}{dt^2} - (mr\sin\theta)\frac{d^2\theta}{dt^2} - mr\left(\frac{d^2\theta}{dt^2}\right)^2\cos\theta + c\frac{dY}{dt} + (\bar{k} + \Delta k \sin \Omega t)Y + \frac{1}{2}\rho D C_D\left|\frac{dY}{dt}\right|\frac{dY}{dt} = 0 \quad (1)$$

$$mr^2\frac{d^2\theta}{dt^2} - mr\sin\theta\frac{dY}{dt} + c_\theta\frac{d\theta}{dt} + k_\theta\theta = 0 \quad (2)$$

A series of quantities can be defined as follows:

$$\omega_y = \sqrt{\frac{k}{M+m}}; \zeta_y = \frac{c}{2(M+m)\omega_y}; \omega_\theta = \sqrt{\frac{k_\theta}{mr^2}}; \zeta_\theta = \frac{c_\theta}{2mr^2\omega_\theta}; m^* = 4\frac{m_s+m}{\rho\pi D^2}; C_a = \frac{4m_a}{\rho\pi D^2}; n = \frac{\Omega}{\omega_y}$$

$$\delta = \frac{\Delta k}{\bar{k}}; \beta = \frac{\omega_\theta}{\omega_y}; y = Y/D; \tau = t\omega_y; \hat{m} = \frac{m}{M}; \hat{r} = \frac{r}{D}; \frac{dY}{dt} = D\omega_y\dot{y}; \frac{d^2Y}{dt^2} = D\omega_y^2\ddot{y}; \frac{d\theta}{dt} = \omega_y\dot\theta; \frac{d^2\theta}{dt^2} = \omega_y^2\ddot\theta \quad (3)$$

being $(\dot{\ })$ the derivative with respect to the nondimensional time τ. Using the above definitions, the dimensionless equations of motion are given by Eqs. 4 and 5.

$$\ddot{y} + 2\zeta_y\dot{y} + (1+\delta\sin(n\tau))y - \frac{\hat{m}\hat{r}}{1+\hat{m}}\left(\ddot\theta\sin\theta + (\dot\theta)^2\cos\theta\right) + \frac{2}{\pi}\frac{C_D}{(C_a+m^*)}\dot{y}|\dot{y}| = 0 \quad (4)$$

$$\ddot\theta + 2\zeta_\theta\beta\dot\theta + \beta^2\theta - \frac{1}{\hat{r}}\sin\theta\ddot{y} = 0 \quad (5)$$

Notice that, for the problem of pure parametric excitation, the dimensionless equation of motion is:

$$\ddot{y} + 2\zeta_y\dot{y} + (1+\delta\sin(n\tau))y + \frac{2}{\pi}\frac{C_D}{(C_a+m^*)}\dot{y}|\dot{y}| = 0 \quad (6)$$

The non-linear hydrodynamic damping is proportional to $|\dot{y}|\dot{y}$ and follows the classical Morison's model. In the context of parametric excitation of risers and TLP tethers, it is responsible for the presence of bounded solutions even in the unstable region of the Strutt diagram ([6]).

Eqs. 4, 5 and 6 were numerically integrated using a Runge-Kutta scheme (ode45 MATLAB® function). The simulations were carried out using time-step $\Delta\tau = 0.01$, $\tau_{max} = 800$ and only two non-zero initial condition, namely $y(0) = 0.1$ and $\theta(0) = \pi/3$.

Results

This paper discusses the effects of three parameters β, $\hat{r}$ and $\hat{m}$ on the suppression of oscillations caused by parametric excitation. The results are discussed from the time-histories of translational and angular displacements ($y(\tau)$ and $\theta(\tau)$ respectively) and the corresponding amplitude spectra.

For the sake of organization, three simulation groups were carried out aiming at identifying the effectiveness of the mentioned parameters in suppressing the cylinder's oscillation. Tab. 1 presents the parameters of each simulation group. The others parameters were kept constant as $\zeta_y = 0.05$, $\zeta_\theta = 0.01$, $\delta = 0.5$, $n = 2$, $C_a = 1$, $C_D = 1.2$, $m^* = 2.6$.

Table 1: Parameters of the different simulation groups.

Group 1			Group 2			Group 3		
β	$\hat{r}$	$\hat{m}$	β	$\hat{r}$	$\hat{m}$	β	$\hat{r}$	$\hat{m}$
$1:4$	0.30	0.50	$1:1$	0.10	0.50	$1:1$	0.30	0.05
$1:2$	0.30	0.50	$1:1$	0.20	0.50	$1:1$	0.30	0.10
$1:1$	0.30	0.50	$1:1$	0.30	0.50	$1:1$	0.30	0.30
$2:1$	0.30	0.50	$1:1$	0.40	0.50	$1:1$	0.30	0.50

Influence of β - Group 1

Time-histories of dimensionless linear and angular displacements (y and θ) and the corresponding amplitude spectra are shown in Fig. 2. Considering firstly the pure parametric excitation case, a steady-state amplitude close to 0.8 with dimensionless oscillation frequency $\hat\omega = \omega/\omega_y = 1$ is reach. Notice that, even with $n = 2$ (principal parametric instability condition), the solution is bounded due to the non-linear hydrodynamic damping.

Now, focus is put on the cases with combined parametric excitation and the internal absorber. Fig. 2(c) reveals a marked decrease in the steady-state oscillation amplitude of response for the cases with $\beta = 1:4$ and $\beta = 1:2$. On the other hand, the cases with $\beta = 1:1$ and $\beta = 2:1$ indicate negligible influence on the dynamics of the cylinder and narrow amplitude spectra.

Considering now the case with $\beta = 1:4$, irregular behaviors can be observed in both $y(\tau)$ and $\theta(\tau)$. Furthermore, such an irregular behavior is more pronounced for $\tau < 400$, where it can be noticed cylinder's oscillations with maximum $y_{max} \approx 0.5$. After $\tau = 400$, this value of β shows to be very effective in the suppression of the cylinder's oscillations, leading to a regime in which practically there is no oscillation of the cylinder, followed by intermittent bursts in which the cylinder reaches a maximum displacement close to 10% of its diameter.

(a) $y(\tau)$.

(b) $\theta(\tau)$.

(c) $y(\tau)$ in the interval $200 < \tau < 250$ and amplitude spectra.

(d) $\theta(\tau)$ in the interval $200 < \tau < 250$ and amplitude spectra.
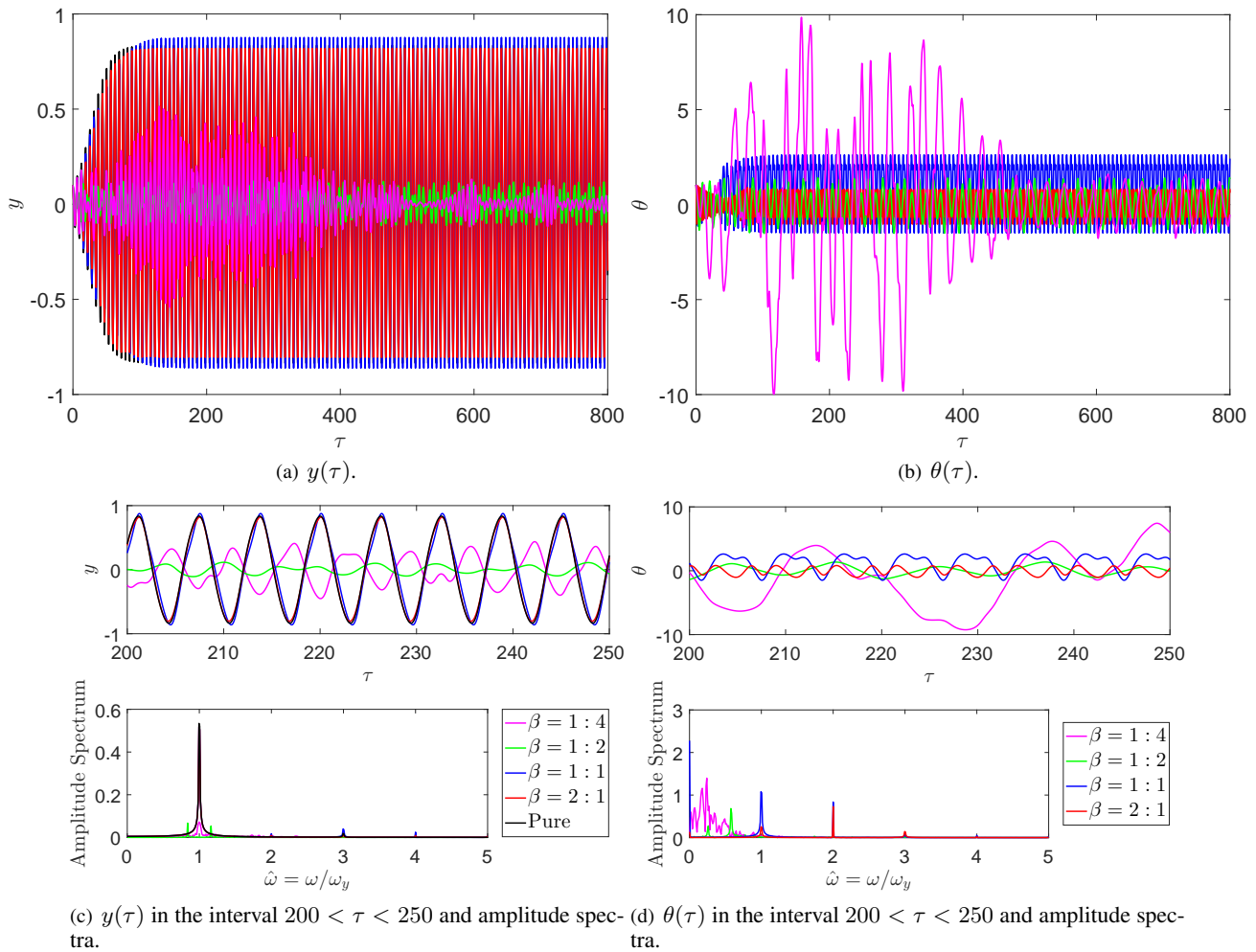
Figure 2: Time-histories and amplitude spectra - Group 1. "Pure" indicates pure parametric excitation.

As already mentioned, the absorber with $\beta = 1 : 2$ is also very effective. This condition leads to a steady-state response with typical amplitude close to 0.1 diameter. Despite this oscillation being larger than that obtained with $\beta = 1 : 4$, there is no burst in the response.

Now, we discuss the angular displacements $\theta(\tau)$ of the internal absorber. As can be seen in Fig. 2(b) and similarly to what is observed for the cylinder's oscillation, irregular response $\theta(\tau)$ is found in the case with $\beta = 1 : 4$ for $\tau < 400$. Curiously, the case with $\beta = 1 : 1$ indicates large oscillations around a non-null value. Notice that, despite the large oscillations of the NES, this condition practically does not lead to a significant decrease in the oscillations of the principal structure.

The amplitude spectra of the angular displacements reveal dominant frequency $\hat{\omega} = 1$ and $\hat{\omega} = 2$ for $\beta = 1 : 1$ and $\beta = 2 : 1$ respectively. The case with $\beta = 1 : 1$ also presents significant energy in $\hat{\omega} = 2$. On the other hand, the condition with $\beta = 2 : 1$ does not show relevant energy in components other than the dominant one.

Influence of $\hat{r}$ - Group 2

Now, focus is put on the investigation of the influence of the length of the NES. For this, Fig. 3 presents the results corresponding to the simulations pertaining to Group 2. One clearly notice from Fig. 3(a) that the cylinder's oscillation is practically not affect by the presence of the internal absorber, despite non-negligible angular oscillations of the NES.

The amplitude spectra presented in Fig. 3(c) corresponding to $y(\tau)$ indicate that all the conditions discussed in the Subsection are narrowbanded and centered at $\hat{\omega} = 1$. It can be also noticed the presence of response at component $\hat{\omega} = 3$ in the case with $\hat{r} = 0.50$.

Now, focus is put on the analysis of $\theta(\tau)$ and the corresponding amplitude spectra. As can be seen in Figs. 3(b) and 3(d), significant angular oscillations are observed for all values of $\hat{r}$. Excepted for the case with $\hat{r} = 0.10$, the time-histories $\theta(\tau)$ present regular behaviors with significant energy at frequencies components $\hat{\omega} = 1$ and $\hat{\omega} = 2$.

Influence of $\hat{m}$ - Group 3

Another aspect investigated in this paper is the influence of the mass of the absorber (or, in dimensionless variables, the influence of $\hat{m}$) on the dynamics of the cylinder. The results corresponding to the simulation Group 3 are presented in Fig. 4(d).

(a) $y(\tau)$.

(b) $\theta(\tau)$.

(c) $y(\tau)$ in the interval $200 < \tau < 250$ and amplitude spectra.

(d) $\theta(\tau)$ in the interval $200 < \tau < 250$ and amplitude spectra.
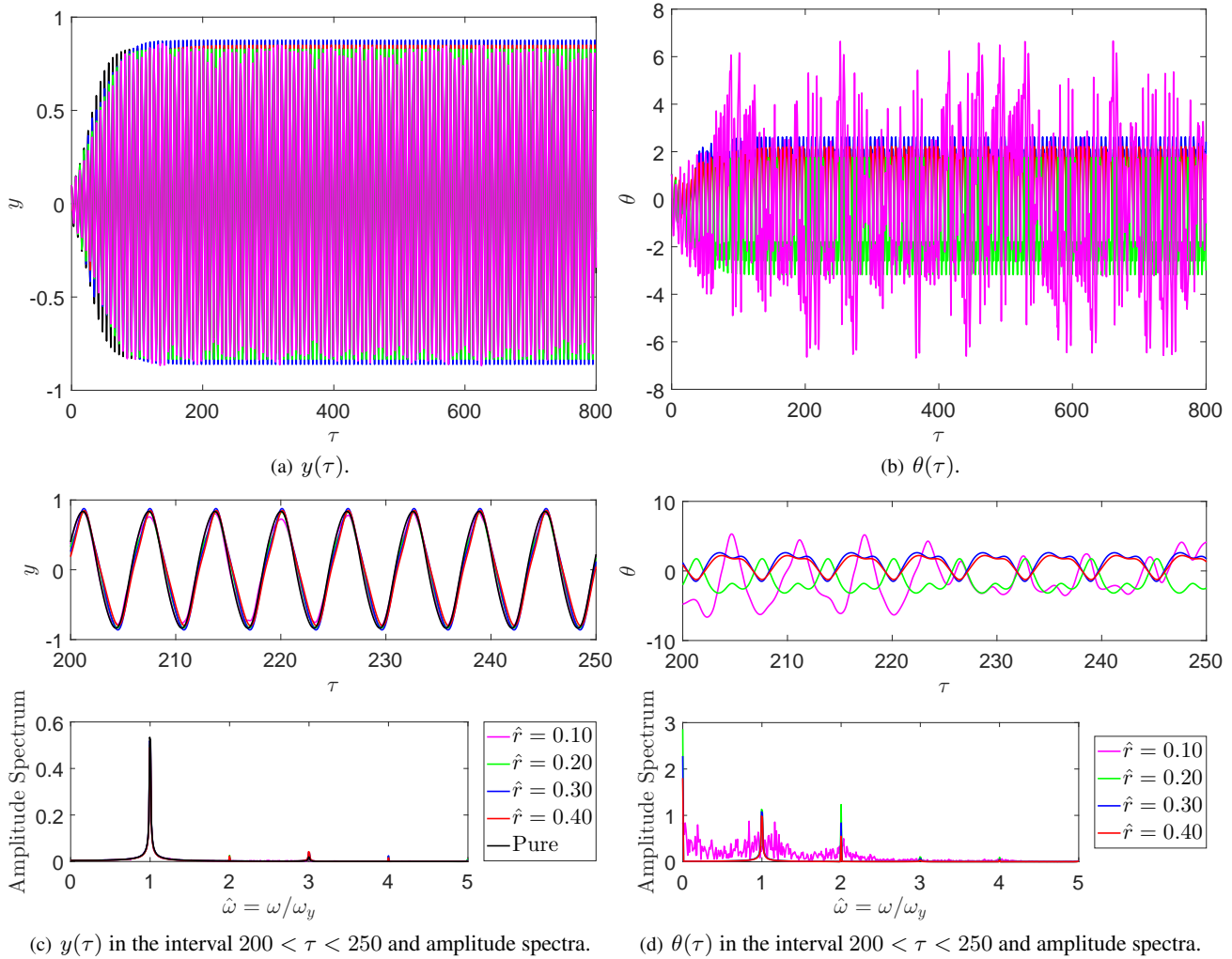
Figure 3: Time-histories and amplitude spectra - Group 2. "Pure" indicates pure parametric excitation.

Similarly to what is found for the simulation Group 2, the values of $\hat{m}$ herein investigated in this Subsection do not lead to a significant decrease in the cylinder's oscillation for the chosen value of β.

Both the quantitative and qualitative aspects of the time-histories $y(\tau)$ are similar to discussed in the previous Subsection, which focused on the influence of $\hat{r}$ for $\beta = 1:1$. All the values of $\hat{m}$ simulated lead to a narrowbanded amplitude spectra centered at $\hat{\omega} = 1$.

The analysis of the time-histories $\theta(\tau)$ reveals a distinct aspect not observed in the analyzes carried out in the others Subsections. In the simulations pertaining to Group 3, steady-state response is obtained for all values of $\hat{m}$.

Also interesting is the behavior of the time-averaged quantity $\bar{\theta}$. Despite the same initial conditions $y(0) = 0.1$ and $\theta(0) = \pi/3$, the cases with $\hat{m} = 0.50$ and $\hat{m} = 0.40$ oscillate around $\bar{\theta} = 1.14$ and $\bar{\theta} = -1.12$ respectively.

Finally, the amplitude spectra evaluated from $\theta(\tau)$ are analyzed. All values of $\hat{m}$ discussed in this Subsection reveal a well-defined peak at $\hat{\omega} = 1$. The cases with $\hat{m} = 0.05$ and 0.10 present similar level of energy at $\hat{\omega} = 0.5$ and 1.5. At frequency component $\hat{\omega} = 2$, energy is found for the cases with $\hat{m} = 0.50$, 0.30 and 0.10.

Poincaré's section

In this Subsection, we discuss the Poincaré's section and projections on the $y(\tau) \times \dot{y}(\tau)$ plane of three simulations, namely the pure parametric excitation case and the conditions with $\beta = 1:4$ and $\beta = 1:2$ pertaining to Group 1. The corresponding time-histories $y(\tau)$ can be found in Figs. 2(a) and 2(c). Herein, Poincaré's sections are obtained for $\tau > \tau_{max}/2$ and using stroboscopic period $T_{sb} = 2\pi$.

The Poincaré's sections and the projections on the $y(\tau) \times \dot{y}(\tau)$ plane are presented in Fig. 5. Considering firstly the pure parametric excitation case, Fig. 5(a) indicates a closed trajectory on the $y(\tau) \times \dot{y}(\tau)$ plane and the Poincaré's sections are collapsed onto a single point. Due to the well known periodic character of parametric excitation response, this aspect is not surprising. One the other hand, Figs. 5(b) and 5(c) reveal very complex trajectories in the considered plane. Furthermore, there is a considerable spreading of the Poincaré's sections, indicating non-periodic responses.

(a) $y(\tau)$.

(b) $\theta(\tau)$.

(c) $y(\tau)$ in the interval $200 < \tau < 250$ and amplitude spectra.

(d) $\theta(\tau)$ in the interval $200 < \tau < 250$ and amplitude spectra.
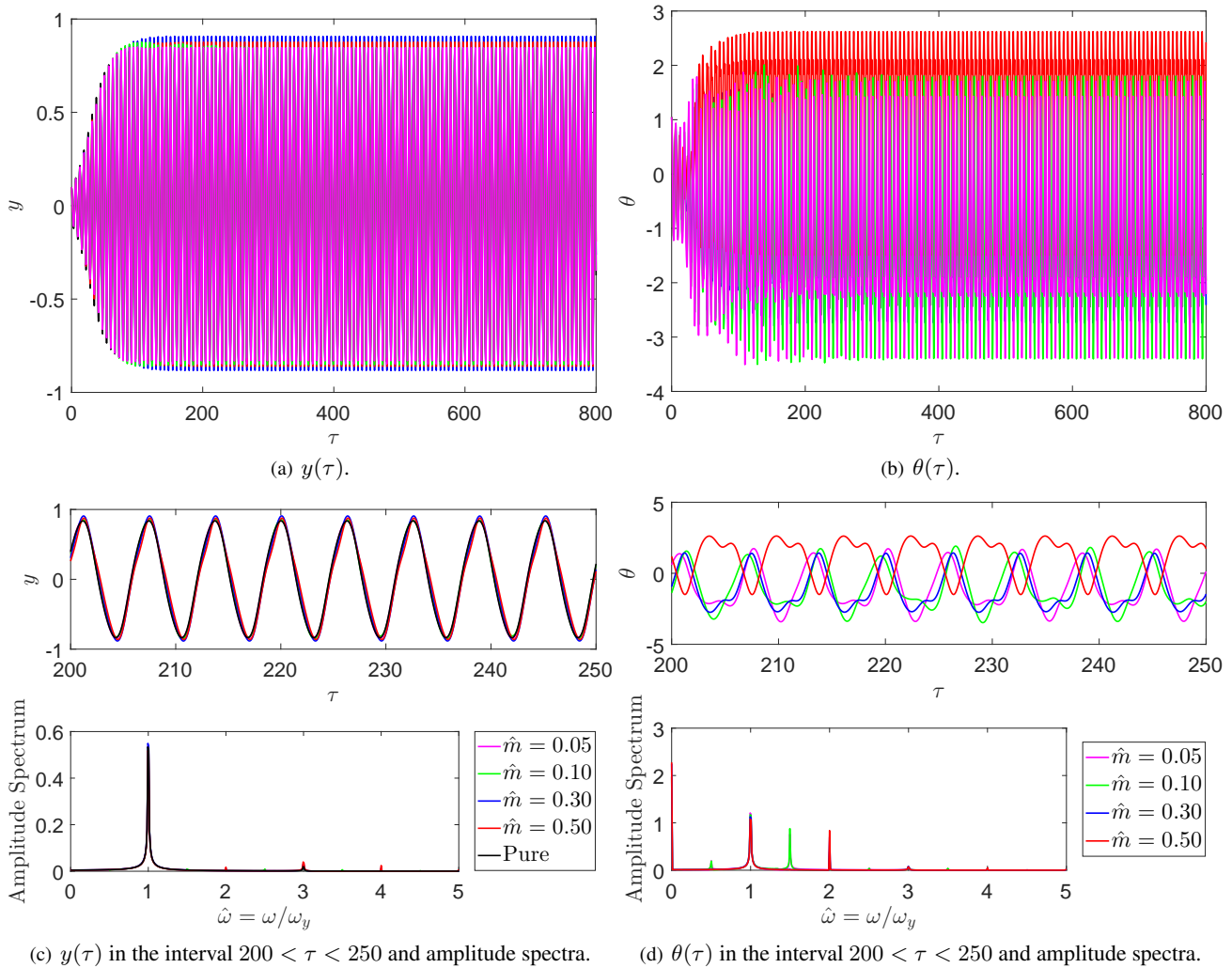
Figure 4: Time-histories and amplitude spectra - Group 3. "Pure" indicates pure parametric excitation.

Conclusions

This paper presented some numerical results from an ongoing research project that focuses on the suppression of oscillations caused by parametric excitation. The passive suppressor herein investigated consisted on a rigid bar, hinged at the cylinder axis and with a tip mass. The dimensionless form of the mathematical model was numerically investigated.

The influence of three parameters of the mathematical model on the suppression of oscillations is investigated. The parametric excitation frequency was chosen to be that corresponding to the principal Mathieu's instability, i.e, twice the natural frequency of the cylinder.

One parameter herein investigated, β, is the ratio between the natural frequencies of the isolated cylinder and absorber. It was found that values of $\beta = 1 : 4$ and $1 : 2$ caused a marked decrease in the cylinder's oscillation amplitude for a certain set of parameters of the mathematical model. On the other hand, fixing $\beta = 1 : 1$, the variation of the length and the mass of the absorber did not present substantial changes in the cylinder's oscillation amplitude. Irregular responses of both the cylinder and the absorber were also found in some conditions.

Further works include a deeper investigation regarding the influence of the parameters of the mathematical model on the suppression of the cylinder's oscillations. Other simulation Groups will be carried out, as well as time-frequency spectral analysis of the time-histories that presented irregular behavior. Asymptotic analysis are also planned aiming at a better understanding of the problem.

Acknowledgments

(a) Pure parametric excitation.

(b) Group 1, $\beta = 1 : 4$.

(c) Group 1, $\beta = 1 : 2$.
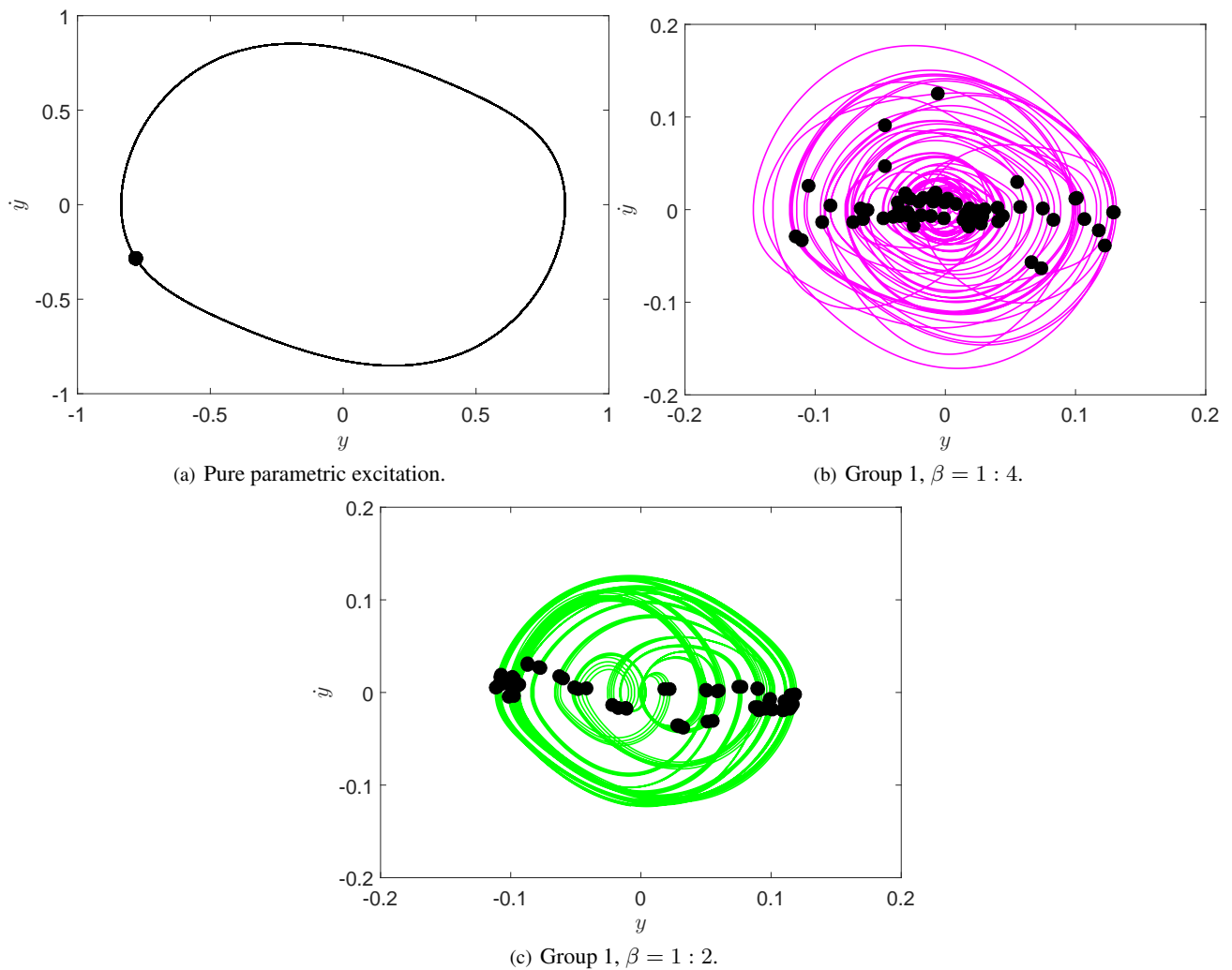
Figure 5: Projections on the $y(\tau) \times \dot{y}(\tau)$ plane and Poincaré's section.

References

[1] Blanchard, A. B.; Gendelman, O. V.; Bergman, L. A.; Vakakis, A. F. (2016) Capture into a slow-invariant-manifold in the fluid-structure dynamics of a sprung cylinder with a nonlinear rotator. *J. Fluid Struc.* **63**:155-173.

[2] Chao, C.-P.; Lee, C.-T.; Shaw, S. W. (1997) Non-unison dynamics of multiple centrifugal pendulum vibration absorbers. *J. Sound Vibr.* **. 204(5): 769-794**.

[3] Issa, J. I.; Shaw, S. W. (2015) Synchronous and non-synchronous responses of systems with multiple identical nonlinear vibration absorbers. *J. Sound Vibr.* **. 348: 105-125**.

[4] Tumkur, R. K. R.; Domani, E.; Gendelman, O. V.; Masud, A.; Bergman, L. A.; Vakakis, A. F. (2013) Reduced-order model for laminar vortex-induced vibration of a rigid circular cylinder with an internal nonlinear absorber. *Commun Nonlinear Sci Numer Sim.* **18**:1916-1930.

[5] Mehmood, A.; Nayfeh, A. H.; Hajj, M. R. (2014) Effects of a non-linear energy sink (NES) on vortex-induced vibrations of a circular cylinder. *Nonlinear dynamics.* **77**:667-680.

[6] Patel, M. H.; Park, H. I. (1991) Dynamics of Tension Leg Platform Tethers at Low Tension. Part I - Mathieu Stability at Large Parameters. *Marine Structures.* **4**:257-273.